A fluorophore-tagged RGD peptide to control endothelial cell adhesion to micropatterned surfaces

LABORATOIRE LIS D'INGÉNIERIE DE SURFACE

Hoesli CA[1,2,3], Juneau PM[3], Chevallier P[1,2], Duchesne C[3], Garnier A[3], and Laroche G[1,2].

[1]*Centre de Recherche sur les Matériaux Avancés, Département de génie des mines, de la métallurgie et des matériaux, Université Laval, Québec G1V 0A6, Canada*
[2]*Centre de recherche du CHU de Québec, Hôpital Saint-François d'Assise, Québec G1L 3L5, Canada*
[3]*PROTEO Research Center and Département de génie chimique, Université Laval, Québec G1V 0A6, Canada*

ABSTRACT
The long-term patency rates of vascular grafts and stents is limited by the lack of surface endothelialisation of the implanted materials. We have previously reported that GRGDS and WQPPRARI peptide micropatterns increase the endothelialisation of prosthetic materials in vitro. To investigate the mechanisms by which the peptide micropatterns affect endothelial cell adhesion and proliferation, a TAMRA fluorophore-tagged RGD peptide was designed. Live cell imaging revealed that the micropatterned surfaces led to directional cell spreading dependent on the location of the RGD-TAMRA spots. Focal adhesions formed within 3 h on the micropatterned surfaces near RGD-TAMRA spot edges, as expected for cell regions experiencing high tension. Similar levels of focal adhesion kinase phosphorylation were observed after 3 h on the micropatterned surfaces and on surfaces treated with RGD-TAMRA alone, suggesting that partial RGD surface coverage is sufficient to elicit integrin signaling. Lastly, endothelial cell expansion was achieved in serum-free conditions on gelatin-coated, RGD-TAMRA treated or micropatterned surfaces. These results show that these peptide micropatterns mainly impacted cell adhesion kinetics rather than cell proliferation. This insight will be useful for the optimization of micropatterning strategies to improve vascular biomaterials.

KEYWORDS
Biomimetic material, cell spreading, endothelialization, micropatterning, surface grafting, vascular grafts

CITATION
Hoesli, C. A., Garnier, A., Juneau, P. M., Chevallier, P., Duchesne, C., & Laroche, G. (2014). A fluorophore-tagged RGD peptide to control endothelial cell adhesion to micropatterned surfaces. Biomaterials, 35(3), 879-890.

This is the author's version of the original manuscript. The final publication is available at Elsevier Link Online via http://dx.doi.org/10.1016/j.biomaterials.2013.09.076

1 INTRODUCTION

Cardiovascular disease is the leading cause of mortality worldwide. Vascular prostheses are used in reconstructive and bypass surgeries when appropriate autologous grafts are unavailable. For small-diameter (< 6 mm) blood vessels such as coronary arteries and low-flow arteries below the knee, the long-term patency rates of vascular prostheses are poor. Intimal hyperplasia at the site of

anastomosis as well as thrombosis lead to the failure of ~60% of small-diameter synthetic grafts within 5 years [1].

Autologous endothelial cell pre-seeding greatly improves the patency rates of small-diameter polytetrafluoroethylene (PTFE) prostheses [2,3], but the procedure is costly and inadequate for emergency situations due to the 2-4 weeks of in vitro cell culture required [4]. To allow endothelial cell adhesion and minimize cell losses after exposure to physiological shear stress, the prostheses are pre-coated with proteins such as fibrin gel [5], collagen [6,7] or fibronectin [8]. However, adsorbing proteins onto prosthetic materials provides little control over their orientation, and hence over their cell receptor binding affinity. Full-length proteins may also progressively lose their activity due to proteolytic degradation. An alternative approach consists in covalently grafting extracellular matrix (ECM)-derived biomimetic peptides onto the synthetic surfaces.

Fibronectin is an ECM protein that is essential for normal vascular development [9] and is involved in angiogenesis during wound healing and tumorigenesis [10-12]. Several fibronectin-derived synthetic peptides promote endothelial cell adhesion, including the GRGDS sequence that contains the integrin-binding RGD domain, as well as the WQPPRARI sequence from the C-terminal heparin-binding domain of fibronectin. The WQPPRARI peptide also enhances haptotactic cell migration [13,14]. The antiapoptotic effects of fibronectin require the presence of the WQPPRARI sequence, which may be due to synergistic survival signals mediated by this sequence and by the RGD motif. Cell binding to fibronectin triggers the exposure of cryptic interaction sites that cause fibronectin aggregation into 5-20 nm diameter fibrils that extend for several mm [15]. The cell-binding domains of individual fibronectin monomers are clustered within these fibrils, creating a network with micropatterned functional domains.

Micropatterned cell-adhesive proteins or peptides can control the organization of the cell cytoskeleton, cell spreading, cell polarity and hence cell fate [16]. The extent of cell spreading on cell-adhesive islands micropatterned over non-adhesive substrates is correlated with decreased rates of cell apoptosis and increased rates of DNA synthesis [17]. Cells can spread across micropatterned cell-adhesive ligands if these are spaced by at most 20-25 mm [18,19]. Well-controlled micropatterned protein or peptide environments can be created by soft lithography or photolithography [20,21]. Applying these techniques to vascular grafts would be challenging since the grafts materials are knitted, woven, extruded or molded to create tubular scaffolds, whereas most lithography methods are applied to 2D surfaces.

We have previously described a scalable air atomization micropatterning method to covalently graft biomimetic peptides onto PTFE surfaces [22,23] that could be adapted to tubular prostheses. Micropatterned GRGDS spots or printed rectangles, in combination with WQPPRARI functionalization of the background surface, increased bovine aortic or human umbilical vein endothelial cell yield after 3 days of culture [22,24]. Micropatterns consisting in 10 mm diameter RGD peptide spots covering 20% of the surface, with the remaining surface functionalized with WQPPRARI led to higher cell yields than surfaces functionalized with a single peptide. However, the local effects of the micropatterns on endothelial cells had not been investigated. In this study, we designed a fluorophore-tagged RGD cell-adhesive peptide that can be efficiently conjugated to aminated surfaces. This peptide was used to visualize aerosol-generated RGD:WQPPRARI peptide micropatterns and their local effects on human saphenous vein endothelial cell (HSVEC) adhesion and expansion.

2 MATERIALS AND METHODS

2.1 Peptides

The CGRGDS (referred to as “GRGDS” since cysteine was not part of the functional fibronectin-derived RGD sequence, but was added to facilitate surface conjugation) and CWQPRRARI (referred to as “WQPPRARI”) peptides were produced by Thermo Fisher Scientific (Waltham, MA), whereas

the fluorophore-tagged GRGDS sequence-containing peptide (referred to as RGD-TAMRA; molecular weight 1437 g/mol) was synthesized and purified by Anaspec (Fremont, CA). The sequence of this peptide is CG-K(PEG3-TAMRA)-GGRGDS-NH_2, where PEG3 represents a three unit-long ethylene glycol spacer grafted onto the side chain of a lysine residue, TAMRA represents the 5-carboxytetramethylrhodamine fluorophore, and -NH_2 represents C-terminal amidation of the peptide. This peptide was resuspended at 2 mM in dimethyl sulfoxide (DMSO, Sigma-Aldrich, St. Louis, MO) and kept frozen until use. Immediately prior to surface conjugation, peptide solutions were prepared by resuspending the peptides at 20 mM in a solution containing 7.5% glycerol added to a 0.2 mm-filtered 10 mM citrate (Sigma-Aldrich) solution at pH 7.4.

2.2 Surface conjugation and micropatterning

Micropatterned glass surfaces were generated using the reaction scheme previously described for Teflon surfaces [22,25], except for the omission of the plasma treatment step and modification of the spray parameters. Commercially available aminated glass slides (treated with aminoalkysilane, Electron Microscopy Sciences, Hatfield, PA) circumvented the need for amination by plasma treatment. To minimize reagent consumption, the circumference of each glass slide was lined with Teflon tape. Each glass slide was covered by 600 mL of a 3 mg/mL suspension of sulfo-succinimidyl4-(p-maleimidophenyl)-butyrate (S-SMPB, Thermo Fisher Scientific, Waltham, MA) in 0.2 mm-filtered calcium-free phosphate buffered saline (PBS, Life Technologies) and incubated for 2 h. Unless otherwise indicated, all reactions were performed with ~50 rpm agitation at room temperature in the dark. The slides were then rinsed in distilled deionized water (dd H_2O), air-dried and stored overnight in the dark. Uniform peptide treatments consisted in the addition of 20 mM solutions of total peptide concentration consisting in either GRGDS alone, WQPPRARI alone, RGD-TAMRA alone, a mixture of GRGDS and WQPPRARI or a mixture of RGDTAMRA and WQPPRARI. To generate micropatterned surfaces, the S-SMPB treated glass slides were placed onto an x-y computer-controlled table (Velmex, Bloomfiel, NY) below the spraying system. This system consisted in a vertically mounted syringe pump (780100C, ColeeParmer Vernon Hills, IL) holding a 250 mL glass syringe (Gastight No 1725, Hamilton Company, Reno, NV) connected to a flat end 22 G needle of 5 cm length introduced into an air atomizing nozzle (SU12SS, Spraying Systems Co., Wheaton, IL) with coaxial air flow at 30 psig. The distance between the needle exit and the glass slide was 21 cm. The entire glass surface was patterned with the atomized peptide solution by 15.8 mm/s motion of the table over 15 cm x-axis distances with 0.5 cm y-axis increments. The syringe pump flow rate was 250 mL/h to obtain w20% surface coverage by the droplets, 500 mL/h to obtain ~35% surface coverage and 750 mL/h to obtain ~50% surface coverage. These conditions are referred to as 20:80, 35:65 and 50:50 peptide patterns when using a GRGDS solution, or 20:80, 35:65 and 50:50 TAMRA patterns when using an RGD-TAMRA solution. The peptide solution droplets were reacted without agitation in a humidified chamber for 3 h. The micropatterned slides were then rinsed in PBS and submerged for 3 h in the WQPPRARI solution. All slides were thoroughly rinsed in PBS and stored for at most 1 month in filtered PBS until use.

2.3 Surface characterization

Static contact angles between deionized water (1 mL) and test surfaces were measured using a VCA 2500 XE system (AST, Billerica, MA). The amine surface concentration on the aminoalkysilane-treated glass slides was quantified through vapor-phase chemical derivatization using 5-bromosalicylaldehyde as described elsewhere [26]. Briefly, the reaction was performed at 85°C for 2 h in a sealed glass tube with a 1 cm-thick bed of soda lime glass beads separating the reagent from the reactive surface. The surfaces were then vacuum-dried overnight at 40°C and analyzed by X-ray Photoelectron Spectroscopy (XPS) with a PHI 5600-ci spectrometer (Physical Electronics, Eden Prairie, MN).

To quantify covalently grafted and adsorbed peptides, glass surfaces were micropatterned with RGD-TAMRA and WQPPRARI, including or omitting the S-SMPB treatment step. These surfaces were then washed and stored in PBS or washed for 2 days in SDSTRIS solution consisting of 0.2 M tris(hydroxymethyl)aminomethane (TRIS, Roche Applied Science, Penzberg, Germany) and 1% sodium dodecyl sulfate (Bio-Rad Laboratories, Hercules, CA) at pH = 11. To determine the surface density of covalently grafted peptides, 0.5 mL droplets containing 1.2 nM to 20 mM RGD-TAMRA were arrayed onto slides with S-SMPB treatment. After 3 h of reaction, the slides were rinsed in PBS, or washed for 2 days in SDS-TRIS solution before storing in PBS. These slides were then imaged by fluorescence microscopy on an Olympus BX51 microscope (Olympus, Tokyo, Japan). In addition, a standard curve consisting of freshly arrayed droplets of the same concentration was also imaged during the same microscopy session using the same exposure time. The fluorescence intensity per RGD-TAMRA molecule was calculated by determining the slope of the total fluorescence intensity with respect to the total molar amount of RGD-TAMRA added per spot in the linear portion of the standard curve. The total fluorescence intensity in the surface-reacted spots was then divided by this value and by the spot area to obtain the surface-reacted RGDTAMRA concentration in molecules/nm^2.

2.4 HSVEC isolation

Healthy saphenous vein segments removed during varicose vein stripping surgeries were obtained with the informed consent of donors at the CHU de Québec, Saint-François d'Assise Hospital in Québec city. All procedures were approved by the CHU de Québec ethics committee. Vein segments were stored in Hank's balanced salt solution (Life Technologies, Carlsbad, CA) until HSVEC isolation. Cells were harvested by rinsing the vein in PBS, introducing 1 mg/mL collagenase type 1A solution (SigmaeAldrich) into the vein and incubating for 15 min at 37°C. The collected cells were harvested and maintained in complete medium containing 20% fetal bovine serum (FBS, Thermo Fisher Scientific), 50 units/mL heparin, 10 ng/ mL basic fibroblast growth factor (bFGF, amino acids 10-155), 50 units/mL penicillin and 50 mg/mL streptomycin in M199 basal medium (all from Life Technologies). The cells were maintained in tissue culture-treated t-flasks (BD Biosciences, Franklin Lakes, NJ) coated for 20 min with 0.2% gelatin (type A from porcine skin, SigmaeAldrich). Cells were frozen in 90% FBS, 10% DMSO freezing medium after the second passage. All experiments were performed with cultures containing >90% von Willebrand factor (vWF) positive cells and using cells at passage 5 or 6.

2.5 HSVEC culture and live cell imaging on functionalized surfaces

Cells washed twice in M199 medium were seeded at 5000 cells/ cm^2 on test surfaces, except for serum-free cell expansion experiments where the cells were seeded at 10 000 cells/cm^2. The test surfaces consisted in functionalized glass slides cut into 2.5 cm by 2.5 cm squares with trimmed corners placed in tissue culture-treated 6-well plates (Sarstedt, Nümbrecht, Germany). Before use, the slides were cleaned and sterilized by 10 min sonication in 95% ethanol (Commercial Alcohols, Markham ON). After 3 h of adhesion, the medium was completed with FBS, heparin, bFGF and antibiotics to culture cells in complete medium for up to 6 days. For serum-free cultures, the M199 medium was removed after 3 h and replaced by serum-free EGM-2 medium. This medium consisted in EBM-2 and Bulletkit supplements (Lonza, Basel, Switzerland), except that the serum supplied in the kit was replaced by 0.4% bovine serum albumin (BSA, Sigma-Aldrich A9647) and insulin, transferrin, selenium (1X ITS, Life Technologies) supplements. Antibiotics (50 units/mL penicillin and 50 mg/ml streptomycin from Life Technologies) were also added. Time-lapse phase contrast and fluorescence images were acquired at 10 to 40 magnification on an automated Olympus IX81 microscope. Between 9 and 25 images per time point per surface were acquired. For live cell imaging on glass test surfaces, 1.5 cm diameter holes were drilled into 6-well plates and glass surfaces were

fastened on top of the drill holes with aquarium silicone glue (Lepage, Henkel, Düsseldorf, Germany). The glue was dried overnight, and the plates were sterilized for 10 min in 95% ethanol before use. At the end of live cell imaging experiments, nuclei were stained with 0.5 mg/mL Hoechst (Life Technologies) added directly to the cultures, followed by fluorescence imaging. Cultures were fixed after 3 h, 3 days or 6 days in 3.7% formaldehyde (VWR International, Radnor, PA) in PBS for 20 min at room temperature and stored in PBS.

2.6 Immunocytochemistry

Fixed cells were permeabilized for 15 min with 0.1% Triton X (VWR) in PBS. After rinsing in PBS, the slides were blocked for 15 min using serum-free protein block (Dako, Glostrup, Denmark) and antibodies against human vinculin (mouse anti-vinculin, SigmaeAldrich) or human vWF (rabbit anti-vWF, SigmaeAldrich) diluted 1:200 in Antibody diluent (Dako) were added. After 1 h at 37 ^{o}C (anti-vinculin) or 2 h at room temperature (vWF), the slides were washed in PBS and incubated for 1 h in the dark with goat anti-mouse Alexa 488 (for vinculin) or goat anti-rabbit Alexa 568 (for vWF) secondary antibodies (both Life Technologies) diluted 1:200 in Antibody diluent. The slides were then stained for 1 h at 37^{o}C with TRITC-phalloidin (SigmaeAldrich) diluted 1:250 in PBS before washing in PBS and dd H_20, followed by staining for 10 min with 1 mg/mL DAPI (SigmaeAldrich) diluted in dd H_2O. The slides were then washed with dd H_2O and PBS, mounted using Vectashield and imaged on an Olympus BX51 microscope.

2.7 Western blotting

Cells were lifted from maintenance cultures using 0.25% TrypsineEDTA (Life Technologies). The trypsin was neutralized by mixing with an equal volume of 0.5 mg/mL soybean trypsin inhibitor (Life Technologies). After washing twice in M199 medium, the cells were seeded at 10 000 cells/cm^2 in M199 medium on functionalized glass slides lined by Teflon tape to create a 10 cm^2 surface. After 3 h, the slides were placed on ice, the medium was removed, and the slides were rinsed with ice-cold PBS. The cells were lysed in RIPA buffer with freshly added 1% phenylmethanesulfonyl fluoride and 1% phosphatase inhibitor cocktail 2 (all from Sigma-Aldrich). After 20 min incubation at 4^{o}C and 300 rpm, the lysate was frozen at 80^{o}C until analysis. Cell lysates were migrated on 4-20% SDS-PAGE tris-glycine gels (Life Technologies) and transferred to a PVDF membrane (Biorad, Hercules, CA). After blocking for 1 h with 5% non-fat dry milk in TBST buffer (50 mM TRIS, 150 mM NaCl from VWR and 0.1% Tween 20 from Amresco, Solon, OH), the membrane was stained overnight at 4^{o}C with 1:500 rabbit anti-pY397 focal adhesion kinase antibody (Life Technologies) or 1:1000 rabbit anti-tubulin antibody (New England Biolabs, Ipswich, MA) diluted in TBST with 5% BSA. The next day, the membrane was incubated in 1:1000 peroxidase-labeled anti-rabbit antibody (New England Biolabs) for 1 h at room temperature. Protein bands were then revealed on an Image Quant™ LAS biomolecular imager (GE Healthcare, Little Chalfont, UK) after staining with Pierce enhanced chemiluminescence 2 substrate (Thermo Fisher Scientific). The membranes were then stripped for 30 min at 50^{o}C in 2% sodium dodecyl sulfate (Biorad, Hercules, CA), 62.5 mM and 0.8% b-mercaptoethanol (Bioshop Canada, Burlington, ON) at pH 6.8. After washing for 30 min under running tap water and rinsing in TBST, the membranes were re-probed overnight in 1:500 rabbit anti-focal adhesion kinase antibody (New England Biolabs) before staining and revealing as described previously.

2.8 Image analysis and cell adhesion kinetics

The cell-covered surfaces (S(t), or degree of confluence) in phase contrast time-lapse images were computed in Matlab® using a range filter of a specified size (RFS), a threshold (MRT) and by filtering out pixel groups smaller than a specified number of pixels (MOST), as described previously

[27]. The algorithm parameters were determined by grid search for each experiment, maximizing the F-measure function for a value of 0.5 (to reach an equal compromise between recall and precision). The performance of the algorithm was assessed by comparing the algorithm output to manually segmented cell-covered surfaces in at least 12 representative ground truth images per experiment. The average F-measure over the entire dataset of calibration images was 0.73 0.12 (standard deviation of 254 images). The average cell area (A(t)) was calculated by dividing the cell-covered surface (S(t)) by the number of cells counted manually in each image (N(t)), and averaging the S(t)/N(t) values of all images taken at a given time t for a given surface. Trends of the average cell area as a function of time were modeled using a general rate equation for a reversible first order reaction:

$$A(t) - A_i = (A_{max} - A_i)\big(1 - exp(-kt)\big) \quad (1)$$

where A_i is the initial cell area, Amax is the maximum cell area determined from the average cell area after 3 h and k is a first order reversible reaction rate constant. This equation is analogous to first order surface adsorption kinetics in liquid/solid systems [28]. This equation can be conceptualized as a highly simplified cell adhesion model where the rate of change in cell area is proportional to the concentration of surface ligands that remain available in the cell vicinity defined as a region surrounding the initial cell area.

In fluorescent images, the cell nuclei, RGD-TAMRA spots and focal adhesions were identified using CellProfiler by correcting the image illumination, enhancing speckles in the case of the focal adhesions, and applying the “Robust background” thresholding method. In Western blot images, protein bands were detected, and their intensities were quantified with ImageJ [29]. The average spot diameter and area of the RGD-TAMRA peptide micropatterns were determined by analyzing >1000 spots per sample surface.

2.9 Cell adhesion kinetics modeling and statistics

Two-way comparisons between samples relied on Student’s t-tests. Unless otherwise mentioned, results represent the average standard error of the mean of 3 experiments. For cell culture experiments, each experiment was performed with cells from a different donor. Multiple group means were compared by ANOVA using the cell donor as a blocking variable, followed by applying the Tukey-Kramer honestly significant difference test. The additive effects of the cell donor, the surface RGD peptide concentration, the type of RGD peptide used and the presence of micropatterns were modeled by least squares linear regression according to Equation (2):

$$E(Y) = \beta_0 + \sum_{j=0}^{j=N_{donors}} \beta_{1j} x_{1j} + \beta_2 x_2 + \beta_3 x_3 + \beta_4 x_4 \quad (2)$$

where β_i and β_{ij} are the model fitting parameters. The variable x_{1j} is a categorical variable representing the cell donor, with a value of 1 attributed to a single donor and all other donors set to 0 for a given experimental data point (i.e. the sum of all β_{1j} will be equal to a single β_{1j}, such as β_{13} for donor 3). The total number of donors (N_{donors}) was 3 for the focal adhesion phosphorylation response and 5 for other response variables (Y). The variable x_2 is a scaled continuous variable representing the fraction of RGD in the solutions reacted with the glass surfaces, x_3 is a categorical variable representing the type of RGD peptide used (GRGDS or RGD-TAMRA) and x_4 is a categorical variable representing the presence or absence of micropatterns. The x_2 variable was scaled between -1 (representing 0% RGD) and +1 (representing 100% RGD) by calculating x_2 = (%RGD-50%)/50%. The term E(Y) represents the expected value of the dependent variable Y. The responses modeled (Y) included the initial rate of cell spreading, the degree of cell spreading after 3 h and the level of focal adhesion kinase phosphorylation, leading to 3 different models of the form

given by Equation (2). The initial rate of cell spreading was determined from the slope of the cell area as a function of time during the first 0.6 h of cell adhesion. The degree of cell spreading after 3 h was determined from the average surface area covered per cell after 3 h of cell adhesion, divided by the average initial cell area. The level of focal adhesion kinase phosphorylation was determined by dividing the pY397 focal adhesion kinase (FAK) band intensity by the β-tubulin band intensity for each sample in Western blots. It should be noted that the experimental design was not adequate to investigate interaction terms, and these were not included to avoid model bias. All statistical analyses were performed using JMP software (SAS Institute, Cary, NC). Results were considered to be statistically significant at $p < 0.05$.

3 RESULTS

3.1 HSVEC adhesion and expansion on non-fluorescent peptide micropatterns

In previous studies with bovine aortic endothelial cells, aerosol-generated GRGDS and WQPPRARI peptide micropatterns increased endothelial cell expansion on PTFE surfaces after 3 days compared to surfaces functionalized with a single peptide. The optimal micropatterns consisted in GRGDS spots of 10 mm average diameter covering 20% of the surface, with the remaining surface functionalized with WQPPRARI. To determine whether these patterns also increased glass surface endothelialisation by human cells, HSVECs were cultured for up to 6 days on functionalized glass surfaces. To obtain the target micropatterns, the aerosol spray flow rate was decreased from 1000 mL/h on PTFE to 250 mL/h on the glass surfaces due to the higher water wettability of aminoalysilane-treated glass (50 ± 5^{o} contact angle after S-SMPB treatment) compared to PTFE (64^{o} contact angle after S-SMPB treatment). Time-lapse phase contrast imaging revealed that the HSVECs spread more rapidly and extensively on surfaces with uniform GRGDS distribution (Fig. 1A). These observations were confirmed by quantifying the initial rate of cell spreading, which was significantly higher on surfaces treated with GRGDS or with a 20:80 GRGDS:WQPPRARI mixture than on the WQPPRARI or the 20:80 micropatterned surfaces (Fig. 1B). The fraction of cells retained on surfaces after fixing at 3 h was $83 \pm 4\%$, with no significant differences between surface treatments. Compared to the untreated surfaces, the micropatterned surfaces led to significantly higher cell expansion after 6 days in serum-containing medium (Fig. 1C). However, no significant differences in cell expansion were observed between the micropatterned surfaces and surfaces with uniform GRGDS and/or WQPPRARI peptide distributions. For the same amount of RGD ligands, the peptide micropatterns therefore reduced the rate of cell spreading without altering the maximum spread cell surface area or subsequent cell proliferation rates.

3.2 Surface micropatterning with a fluorophore-tagged RGD peptide

To observe the local effects of peptide micropatterns on HSVECs, a fluorophore-tagged RGD peptide was designed (Fig. 2A). To avoid steric hindrance of integrin binding to the RGD site, the TAMRA fluorophore was placed on a polyethylene glycol spacer arm (17.8 °A nominal length) linked to a lysine side chain (6.41 °A nominal length). This added lysine residue was placed upstream from the RGD sequence and flanked by two glycine residues to increase chain flexibility. To create an anchorage point to the S-SMPB treated surface, a cysteine residue was added at the N-terminus of the peptide chain. The C-terminus of the peptide was amidated to reflect the non-terminal location of the peptide within fibronectin, although this was not expected to significantly change integrin binding affinity [30]. This RGD-TAMRA peptide was reacted with aminoalkysilane and S-SMPB treated glass surfaces. Fig. 2B shows the RGD-TAMRA surface concentration obtained after this reaction scheme compared to unreacted peptide standards. Based on XPS analysis, the relative amount of primary amine moieties on the glass surfaces before S-SMPB treatment was 5.4%. In previous studies of the surface amine content of plasma-treated PTFE, we determined that 2-3.5%

amine surface concentrations correspond to 0.5 to 2 amine groups/nm^2 [24]. Based on this estimate, the XPS data suggests that the amine surface concentration should be between 0.8 and 5.4 amine groups per nm2. After S-SMPB treatment and reaction with 20 mM RGD-TAMRA, the surface concentration of RGD-TAMRA residues was 0.223 0.002 RGD-TAMRA molecules/nm^2 based on fluorescence measurements. It is possible that unreacted amine groups remained on the surfaces but were inaccessible for further reaction due to steric hindrance by the surface-conjugated RGD-TAMRA. The concentration of the unreacted RGDTAMRA solution was in large excess over both the primary amine surface concentration before reaction and the final covalently grafted RGD-TAMRA surface concentration. In the absence of SSMPB, no significant TAMRA fluorescence was detected on the surfaces after washing with detergent. Fig. 3A shows the fluorescent micropatterns observed after spraying RGD-TAMRA onto the surface at different flow rates and reacting the remaining surface with WQPPRARI. Increasing the RGD-TAMRA spray flow rate from 250 mL/h to 500 mL/h or 750 mL/h significantly increased the surface area covered by spots from 21 3% to respectively 37 $\pm$ 4% or 48 $\pm$ 1%. These values also correspond to the average area under the curve in Fig. 3B. Surfaces treated with uniform peptide mixtures were reacted with solutions containing 20:80, 35:65 and 50:50 RGD-TAMRA:WQPPRARI peptide ratios, which are not significantly different from the ratios present on the patterned surfaces. To simplify the notation, the micropatterning conditions described above were referred to as 20:80, 35:65 and 50:50 TAMRA micropatterns. For the 20:80 TAMRA micropatterns, the average spot diameter was 9 $\pm$ 1 mm. The average spot area was 608 $\pm$150 mm^2, corresponding to an average area-based spot diameter of 28 $\pm$ 14 mm, which is a more relevant indication of the average spot size cells contacted during cell adhesion. No significant differences in the average spot area were observed for the 35:65 and the 50:50 TAMRA micropatterns. These results show that fluorophore-tagged RGD micropatterns with reproducible spot densities can be obtained using the aerosol-based technique.

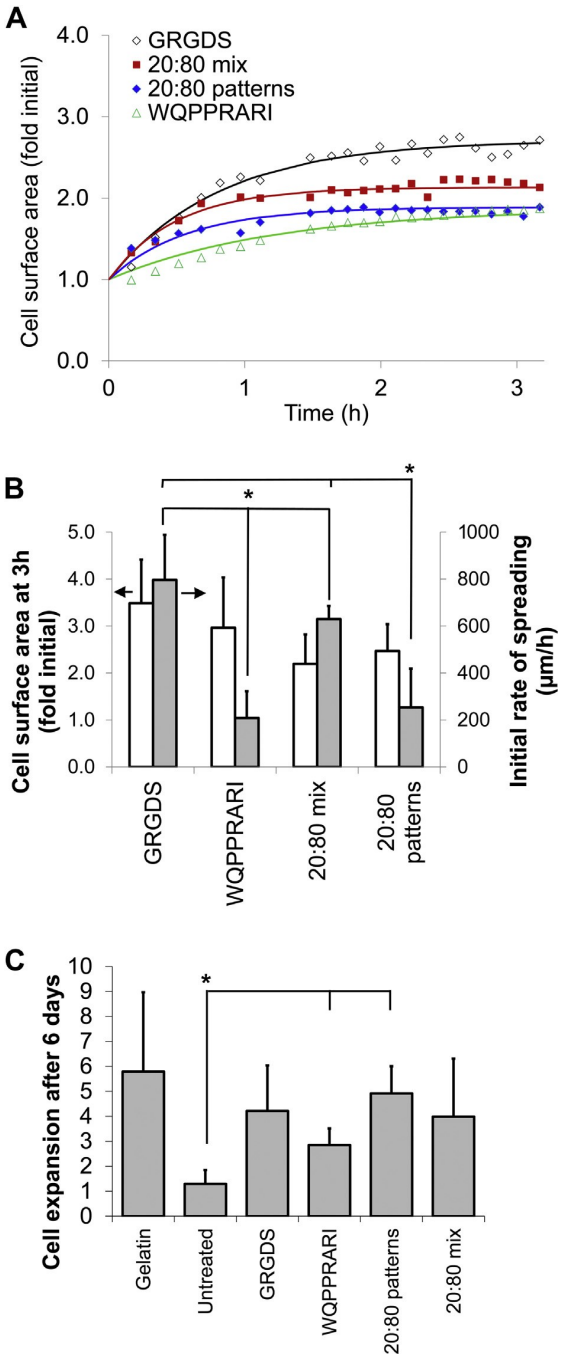

Figure 1. Cell spreading and growth on functionalized surfaces. Surfaces were functionalized with WQPPRARI, GRGDS, 20:80 GRGDS:WQPPRARI micropatterns or a 20:80 mixture of the two peptides. A) Change in the average cell surface area during the first 3 h after seeding, modeled by first order reversible reaction rate kinetics (Equation (1)). The data from one experiment is shown. B) Ratio of the average final cell surface area after 3 h to the initial cell area measured in each experiment (white bars) and initial rate of cell spreading (gray bars). Note that the average initial cell area of 5 donors was 603 ± 8 mm^2. C) Cell yield after 6 days of culture in serum-containing medium. *$p < 0.05$ compared to the condition aligned with the "*" symbol. Note: in (C), the comparisons are based on paired t-tests, whereas no significant difference was identified following Tukey's range test for multiple comparisons.

3.3 Cell adhesion on fluorophore-tagged peptide micropatterns

Next, the effects of the fluorophore-tagged peptide micropatterns on cell adhesion were examined by time-lapse imaging. First, HSVEC adhesion was monitored side-by-side on surfaces treated with GRGDS alone or RGD-TAMRA alone to determine whether the cell binding activity was conserved with the TAMRA-tagged peptide. Surprisingly, HSVEC spreading was faster and more extensive on the RGD-TAMRA surfaces than on the GRGDS surfaces (Movie 1). Within 30 min on RGD-TAMRA surfaces, the cells returned to cobblestone morphologies typical for endothelial cells, contrary to cells on the GRGDS surfaces. The binding affinity between cell integrins and the RGD sequence therefore appeared to be higher for surface-conjugated RGD-TAMRA than for the GRGDS peptide. On the micropatterned surfaces, local effects of the RGDTAMRA micropatterns on cell adhesion were observed (Movie 2).

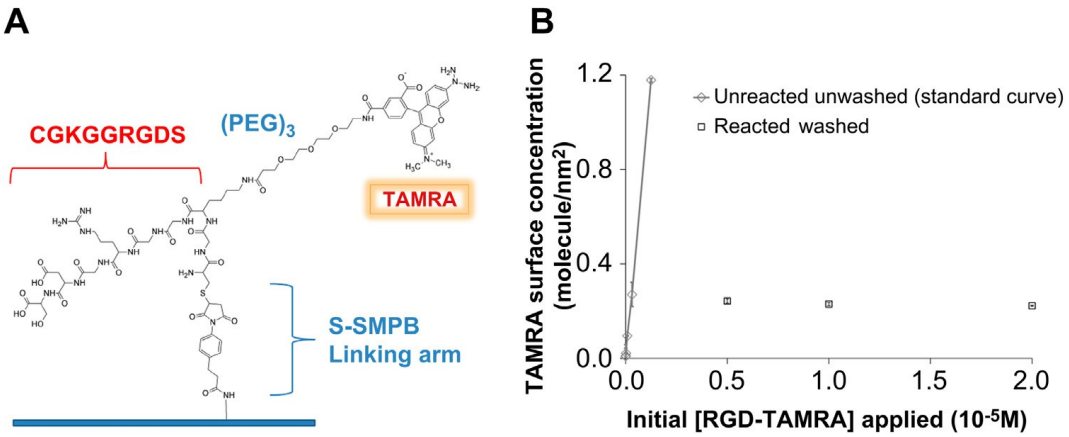

Figure 2. Surface conjugation of the TAMRA fluorophore-tagged RGD peptide. A) Final molecular structure of the RGD-TAMRA peptide covalently reacted with aminosilane glass surfaces using the bi-functional sulfo-SMPB linking arm. B) RGD-TAMRA surface concentration before and after reaction of 0.5 mL droplets on the surfaces. The surface concentration was calculated by relating the total fluorescence intensity per nm^2 droplet surface to known concentration standards.

Pseudopod extension was guided by the neighboring RGD-TAMRA spots, leading to non-uniform cell spreading, contrary to surfaces with uniform RGD-TAMRA distributions. During cell spreading, cell pseudopods that contacted the RGD-TAMRA spots continued to extend or were retained on the spots but were retracted from WQPPRARI regions. Actin polymerization was observed during cell adhesion using an actin-GFP fusion protein. After 3 h of cell adhesion to the micropatterned surfaces, most actin filaments spanned cell regions between the RGD-TAMRA spots, while few filaments were observed within the spots (Movie 3). The actin filaments appeared to be anchored at the periphery of the RGD-TAMRA spots. The actin-GFP protein was also concentrated in membrane ruffles at the cell periphery. Supplementary data related to this article can be found online at http://dx.doi.org/10.1016/j.biomaterials.2013.09.076.

Quantitative analysis of the rate and extent of cell spreading confirmed the qualitative observations from time-lapse movies. Fig. 4A shows characteristic curves representing the change in cell area as a function of time during cell adhesion. A rapid increase in cell surface area was noted within the first 30 min of adhesion on surfaces functionalized with RGD-TAMRA, RGD-TAMRA:WQPPRARI micropatterns or a mixture of the two peptides. The initial rate of cell spreading measured over this time period was significantly higher on the RGD-TAMRA and 35:65 TAMRA micropatterned surfaces than on surfaces with WQPPRARI (Fig. 4B). It should be noted that the

image analysis algorithm overestimated the cell surface area for surfaces with low cell spreading (e.g. WQPPRARI) and underestimated the cell area on surfaces with high cell spreading (e.g. RGD-TAMRA) based on the mean signed differences between the estimated areas and the areas in ground truth images. This can be explained by the fact that the model parameters were set to minimize the relative error over all surface types, which may lead to increased bias for surfaces leading to cell phenotypes different from the average cell phenotype. As a consequence, the differences observed between different surfaces in Fig. 4 may be conservative.

As expected from the time-lapse imaging experiments, HSVECs formed focal adhesions within 3 h on the micropatterned surfaces, as well as other surfaces reacted with RGD-TAMRA (Fig. 5). The number of focal adhesions per cell was 221 ± 47 on RGD-TAMRA treated surfaces, 47 ± 11 on WQPPRARI-treated surfaces, 143 5 on surfaces treated with a 35:65 mixture of the two peptides and 108 ± 8 on the micropatterned surfaces. Few focal adhesions were visible on the WQPPRARI-treated surfaces (Fig. 5) or gelatinized surfaces (not shown). On surfaces with uniform RGD-TAMRA distribution, the focal adhesions were uniformly distributed near cell edges. On the micropatterned surfaces, most (73 ± 2% for the 35:65 TAMRA patterns) of the focal adhesions were co-localized with the RGD-TAMRA spots, and they were concentrated near spot edges. Increasing micropattern densities (20%, 35% or 50% surface coverage by RGD) appeared to lead to increasing levels of cell spreading (Fig. 5). However, this observation in fixed cell samples was not reflected by statistically significant differences in phase contrast images. In the absence of statistically significant effects between different patterning densities, further experiments were conducted with the 35:65 TAMRA patterns.

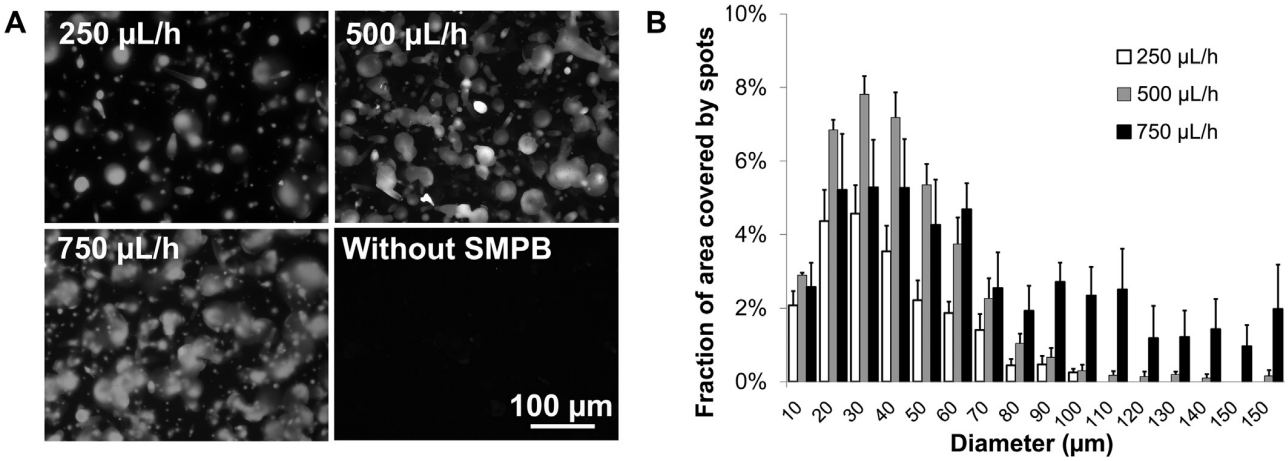

Figure 3. RGD-TAMRA/WQPPRARI micropatterns generated using different RGD-TAMRA spray flow rates. A) Fluorescence photomicrographs of the surface-conjugated RGD-TAMRA patterns obtained. B) Size distribution of the RGD-TAMRA spots with respect to the fraction of the total surface area covered by spots of a given size.

To confirm that focal adhesion formation led to the activation of downstream signaling cascades, phosphorylated Y397 focal adhesion kinase (FAK) was quantified (Fig. 6). FAK is a scaffolding protein that is recruited to sites of integrin clustering, which leads to FAK trans-autophosphorylation on Y397 and subsequent recruitment of SH_2 proteins that activate other kinases and phosphatases. After serum starvation and detachment from surfaces, the levels of Y397 phosphorylated FAK (pY397 FAK) in HSVECs were nearly undetectable by Western blot. After 3 h of cell adhesion, pY397 FAK was activated on all of the biomimetic materials (Fig. 6A). The pY397 FAK/β-tubulin ratio was significantly higher on the 35:65 TAMRA mix surfaces than any of the surfaces without TAMRA. It should be noted that although the total FAK levels appeared to be elevated in the 35:65 TAMRA mix and patterned conditions, no significant changes between conditions were quantified. There were

also no significant differences in pY397 FAK/b-tubulin ratio between the 35:65 TAMRA patterns, the 35:65 TAMRA mix and the RGD-TAMRA conditions. Moreover, the presence of 35% RGDTAMRA on the surfaces (i.e. 0.35 x 0.2 ≈ 0.07 molecules/nm^2 for the 35:65 mix surfaces) was sufficient to elicit similar pY397 FAK/β-tubulin ratios as controls coated with gelatin and supplemented with serum. This striking increase in pY397 FAK/b-tubulin ratio and the lack of further increase on 100% RGD-TAMRA surfaces suggests that this RGD-TAMRA surface concentration was sufficient to reach maximal surface-dependent FAK phosphorylation, both with uniform and patterned RGD distributions.

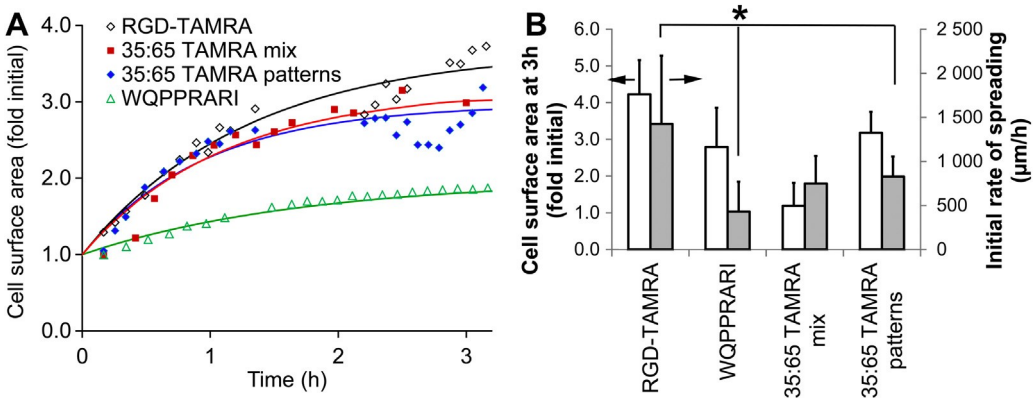

Figure 4. Endothelial cell spreading on fluorophore-tagged micropatterned surfaces and controls. A) Change in the average cell surface area during the first 3 h after seeding, modeled by first order reversible reaction rate kinetics (Equation (1)). The data from one experiment is shown. B) Ratio of the average final cell surface area after 3 h to the initial cell area measured in each experiment (white bars) and initial rate of cell spreading (gray bars). *p < 0.05 compared to the condition aligned with the "*" symbol.

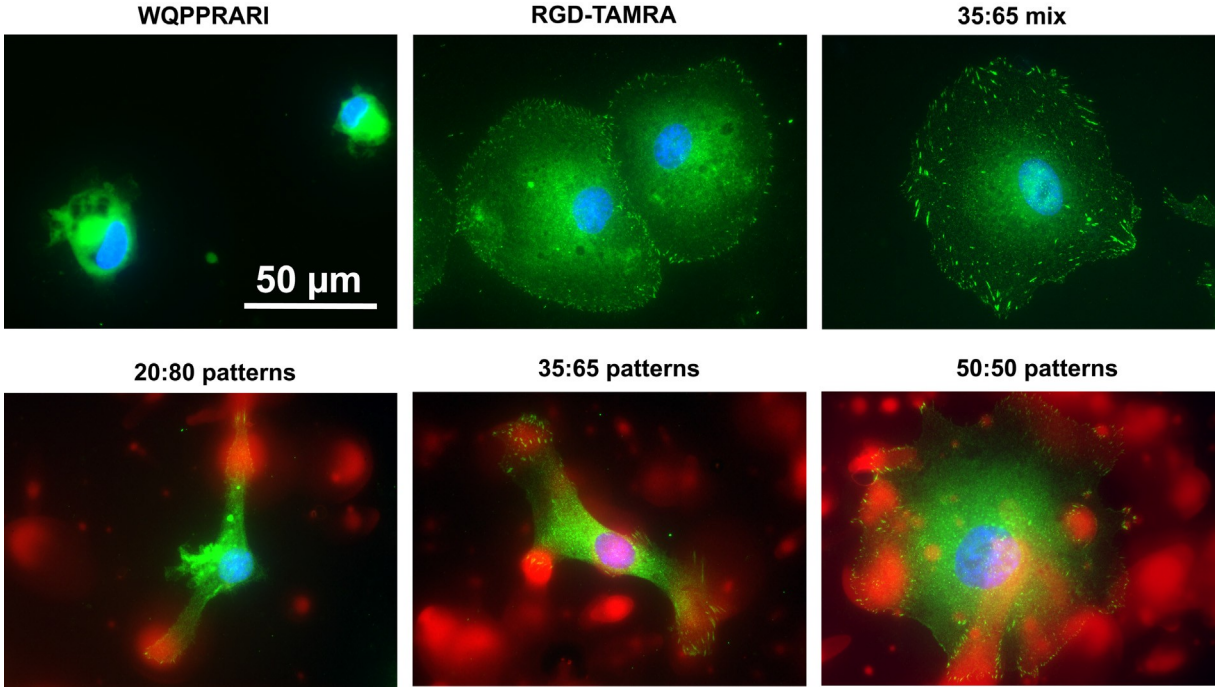

Figure 5. Effect of peptide surface grafting on the distribution of focal adhesions. HSVECs were fixed after 3 h of adhesion. Vinculin staining is shown in green, RGD-TAMRA patterns are shown in red and DAPI nuclear staining is shown in blue. Surface were functionalized with WQPPRARI, RGD-

TAMRA, a 35:65 mixture of RGD-TAMRA:CWQPPRARI or micropatterned to obtain either 10%, 35% or 50% RGD-TAMRA surface coverage with WQPPRARI (dark background) reacted with the remaining surface. The red channel was omitted from the “RGD-TAMRA” and “35:65 mix” panels. (For interpretation of the references to color in this figure legend, the reader is referred to the web version of this article.)

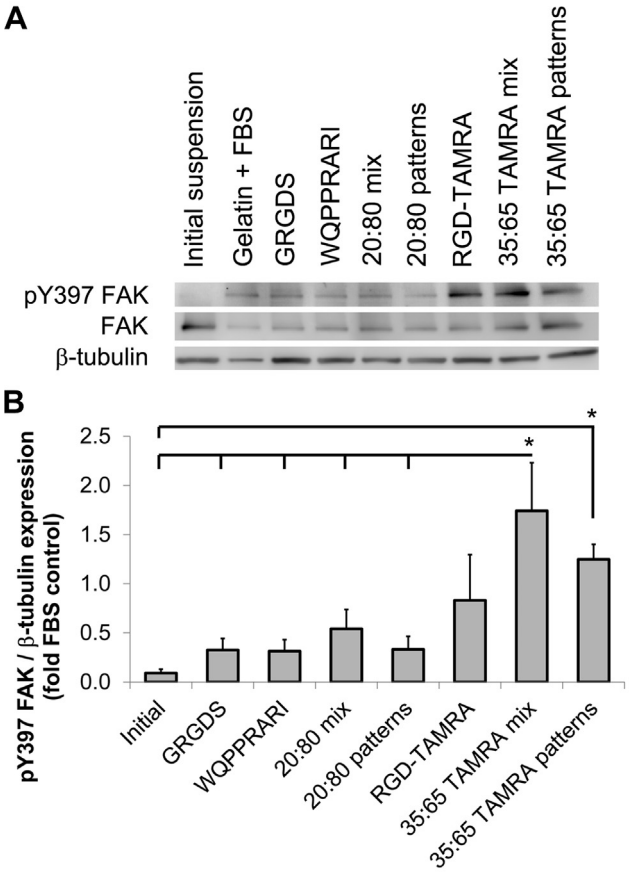

Figure 6. Effect of functionalized surfaces on focal adhesion kinase phosphorylation. HSVECs were cultured in serum-free medium overnight, resuspended for 1 h in basal medium and then seeded in basal medium on test surfaces. As a positive control, cells were seeded in complete medium with 20% FBS on gelatin-coated surfaces. After 3 h, the cells were lysed and pY397 FAK, total FAK and b-tubulin were quantified by Western blot. Note: the results shown are from a single HSVEC culture, with the results from 2 further cultures pending. *$p < 0.05$ compared to the 35:65 TAMRA mix or micropatterned surfaces.

Finally, a multifactorial model was applied to quantify the relative importance of the main effects of the RGD surface concentration, of using RGD-TAMRA instead of the GRGDS peptide and of surface patterning. The responses modeled were the change in cell surface area after 3 h of adhesion, the initial rate of cell spreading and the pY397/b-tubulin ratio. This model also included the donor cell source as a main effect, since high variability between experiments was observed. This overall model (Fig. 7) therefore summarizes the findings shown in Figs. 1, 4 and 6. This global model revealed that taken together, only the use of RGDTAMRA instead of GRGDS significantly affected the rate and extent of cell spreading, and FAK autophosphorylation. In Figs. 1 and 4, the RGD:WQPPRARI ratio was found to significantly alter the rate of cell spreading and FAK phosphorylation, but the added variability from combining all the collected data reduced the significance of this effect. This model indicated that RGD-TAMRA lead to a pronounced increase in

cell integrin affinity for the biomimetic surfaces, which largely surpassed the effect of the GRGDS peptide concentration alone. At 35% RGD-TAMRA surface coverage, the micropatterns did not significantly affect the rate of cell spreading, but the orientation of cell spreading was guided by neighboring patterns. The RGD-TAMRA micropatterns can therefore be used to control cell morphologies while providing similar matrix-cell signals as uniformly distributed cell adhesion peptides.

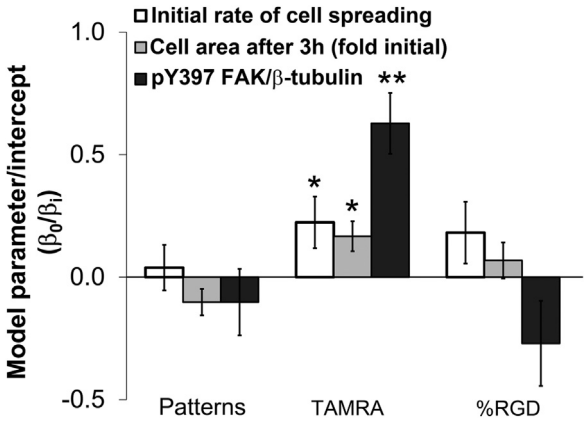

Figure 7. Surface effects on the rate and extent of cell spreading, and FAK phosphorylation. The linear model described by Equation (2) was applied to the different dependent variables (Y values, indicated in the legend). The main effects of four independent variables were modeled: the cell donor (x_{1j}), the presence of micropatterns on the surface (x_2), the type of cell adhesion peptide used (GRGDS or RGD-TAMRA, x_3) and the fraction of RGD-containing peptides on the surface (x_4). The values of the model parameters corresponding to the effects of these variables (β_i) are reported relative to the model intercept for each read-out (β_0). The model parameters associated with the cell donor are not shown, but the donor effects were statistically significant and the β_{1j}/β_0 values ranged between -0.65 ± 0.2 and 1.14 ± 0.2. *$p < 0.05$, **$p < 0.001$.

3.4 Cell expansion on fluorophore-tagged peptide micropatterns

As expected from the previous results with GRGDS:WQPPRARI (Fig. 1C), the RGD-TAMRA:WQPPRARI micropatterned glass surfaces led to higher levels of endothelialisation than untreated surfaces (Fig. 8A). Similar to cell adhesion kinetics, there were no significant differences in cell expansion between patterned or uniform RGD-TAMRA distribution. During the adhesion experiments, adhesion to the RGD-TAMRA containing surfaces led to FAK activation in the absence of serum. Since FAK activation can trigger activation of the mitogen-activated protein kinase pathway and cell proliferation, the potential of the biomimetic surfaces for serum-free cell expansion was tested (Fig. 8B). Contrary to untreated surfaces, significant cell expansion was observed on the RGDTAMRA functionalized surfaces. The serum-free cell expansion obtained on RGD-TAMRA was ~2/3 the cell expansion quantified on gelatin. This result indicated that primary HSVECs can be cultured in defined surface and medium conditions on RGD-TAMRA functionalized surfaces. On the 35:65 TAMRA patterned surfaces, no significant colocalization between the RGD-TAMRA spots and focal adhesions was observed after 3 days of cell expansion. The patterns also did not appear to impact cell shape or membrane extensions during serum-free cell culture (Movie 4), including during cell division events (Movie 5). On a cautionary note, cells cultured in serum-free medium grew as clustered elongated cells, contrary to the well-spread cobblestone phenotype of endothelial cells in serum-supplemented medium. The reduced size and vinculin staining intensity of focal adhesions in serum-free medium also suggested reduced maturity or higher turnover of focal adhesions in the absence of serum. Supplementary data related to this article can be found online at

http://dx.doi.org/10.1016/j.biomaterials.2013.09.076. Overall, the trends observed in both the cell adhesion experiments and in cell expansion experiments are consistent with increased cell-surface interactions on surfaces with RGD-TAMRA, including the micropatterned surfaces. Peptide micropatterning using RGD-TAMRA constituted a unique tool to identify the location of peptides in live cell imaging experiments. This approach confirmed significant effects of peptide micropatterns on cell morphology and focal adhesion formation during cell adhesion, without affecting FAK activation and the rates of cell spreading or proliferation.

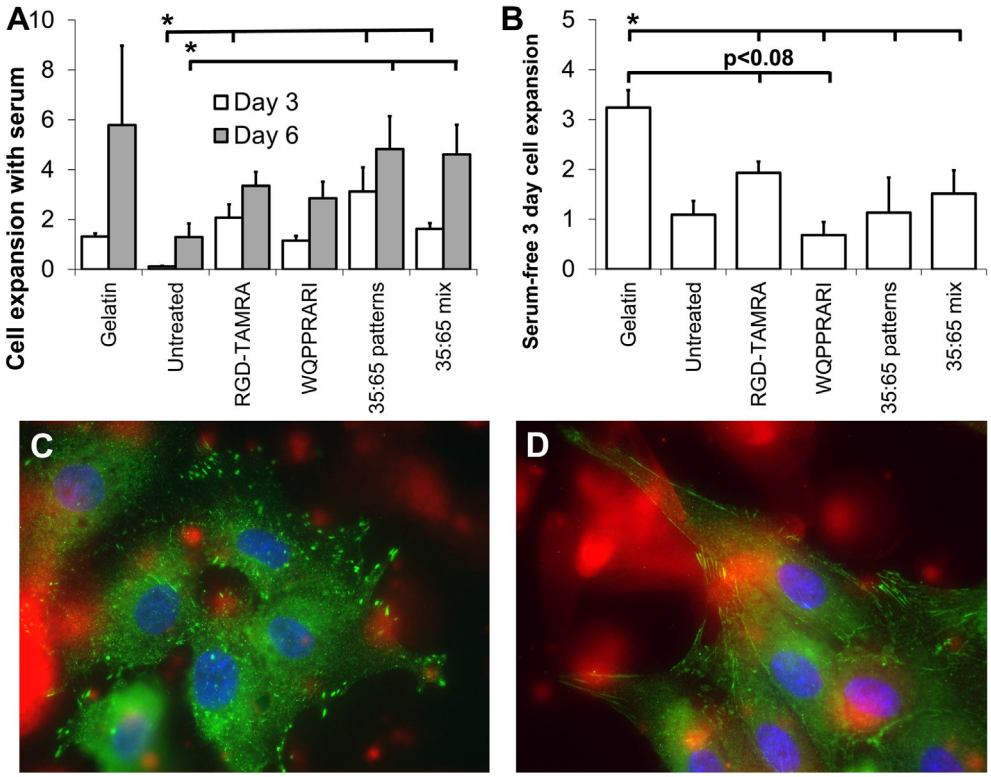

Figure 8. Cell expansion on RGD-TAMRA functionalized surfaces in serum-free medium. A) Cell expansion (cell number on day 3 or day 6/initial cell number) in serum-free or B) serum-containing medium based on DAPI-stained nuclei enumeration. C and D) Distribution of focal adhesions observed after 3 days on RGD-TAMRA functionalized surfaces in serum-containing (C) or serum-free (D) media. *p < 0.05 compared to the condition aligned with the "*" symbol, except in B, where conditions with p-values <0.08 compared to RGD-TAMRA are also indicated. The number of replicate experiments (with separate donors for each experiment) was N = 4 for B.

4 DISCUSSION

The surface modification of synthetic vascular grafts with biomimetic peptides is a promising simple strategy to improve graft endothelialisation and long-term performance. In this study, we characterized the effects of surface-conjugated fibronectin-derived peptide micropatterns on endothelial cell adhesion and proliferation kinetics. The micropatterns significantly affected cell morphology and the localization of focal adhesions, without altering the extent of cell spreading or proliferation. The micropatterns consisted in ~10 mm diameter RGD peptide spots that guided pseudopod orientation and focal adhesion formation, surrounded by a WQPPRARI background that improved cell expansion compared to bare surfaces (Fig. 1C). Although the RGD spots only covered a fraction of the surface (e.g. 35%), the micropatterned surfaces led to similar levels of FAK Y397

phosphorylation as surfaces with 100% RGD surface coverage. The peptide micropatterning strategy therefore affords control over cell shape and orientation, while avoiding anoikis and allowing similar levels of cell expansion as surfaces with uniform distributions of peptide mixtures.

The main advantage of the aerosol-based micropatterning method is that it could be adapted to pattern tubular structures such as commercially available vascular prostheses or other tubular vascular devices. Another unique feature of the micropatterning strategy described here and in our previous work [22,23,25,31] was the use of combinations of peptides rather than micropatterning a single peptide or protein. In this case, the surfaces were patterned with peptides containing the GRGDS cell adhesion-promoting sequence, while the remaining surface was reacted with the cell motility-enhancing WQPPRARI peptide. The surface conjugation strategy led to ~0.2 molecules/nm^2 peptide concentrations, or w1 nm mean random distance between the surface-grafted molecules. For the 35:65 peptide micropatterns, the mean random distance calculated between spot centers was 7.5 mm. In vivo, fibrillogenesis leads to the cell-mediated reorganization of fibronectin into clustered fibrils of mm-scale length [32] with repeating units spaced by ~71 nm [33]. The micropatterns generated by the aerosol technique therefore approach the length scales between fibronectin fibrils in the ECM, but not the nanoscale-level clustering of RGD and WQPPRARI residues within clustered fibrils. To further enhance surface biomimetism, it would be interesting to study the combined effects of nanoscale clustering [34-36] and micropatterning on cell adhesion and cell fate. On the other hand, one drawback of the aerosol technique was that the random distribution of the aerosol-generated spots complicated the identification of regions reacted with each peptide. One approach to overcome this challenge was to develop well-characterized fluorophore-tagged peptides that would enable more refined analysis of the effects of the micropatterns on cell behavior.

To uncover the local effects of the peptide patterns on endothelial cell spreading and proliferation, we designed a TAMRA fluorophore-tagged RGD-containing peptide that allows live cell imaging of cell-peptide interactions. This peptide was efficiently conjugated to activated aminated surfaces through simple maleimide-thiol coupling chemistry. One surprising finding was that this RGD-TAMRA peptide significantly increased the rate and extent of endothelial cell adhesion compared to the original GRGDS sequence. The RGD-TAMRA peptide also led to significantly higher levels of FAK Y397 phosphorylation. Both of these peptides contain the GRGDS cell-adhesive sequence, but the RGD-TAMRA peptide contains 3 additional N-terminal amino acids. These amino acids include two glycine residues flanking a lysine residue with a PEG3 spacer and the TAMRA fluorophore conjugated to the lysine side chain. The enhanced integrin binding affinity of this surface-conjugated peptide compared to the GRGDS peptide could therefore be explained by the increased distance between the cell-binding sequence and the surface, the increased chain flexibility provided by the added glycine residues and/or changes in the electronic environment of the cell-binding sequence. The presence of different spacer arms between a solid support and affinity binding molecules can affect the interactions between these molecules and their binding partners. The effect of the spacer length has been well-studied in the context of microarray technologies [37,38] and the targeting of nanoparticles to desired tissues [39,40]. The conformation of the RGD sequence and the residues surrounding this sequence impact its integrin binding affinity [41] and its effect on cell adhesion [42]. For instance, the presence of two sequential glycine residues preceding the RGD sequence or the presence of the large PEG3-TAMRA group may have favored higher affinity conformations similar to those found in cyclic RGD peptides. Lastly, changes in the electronic environment, for example through the addition PEG groups, can change the preferential conformations of small charged peptides [29,43].

The RGD-TAMRA micropatterns revealed that most of the focal adhesions formed within 3 h were localized on the RGD spots, particularly at spot edges. This observation is consistent with the reported increase in focal adhesion strength and maturation where higher tensional forces are applied on the substrate [16,44]. Actin filaments formed between but not within the RGD spots (Movie 3), reminiscent of observations made with adhesive islands printed over non-adhesive substrates [45]. Changes in the micropattern density from 20% to 35% or 50% surface coverage by

the RGDTAMRA spots did not significantly impact cell spreading or expansion kinetics. However, these changes did significantly impact cell shape, progressively leading to more uniform spreading rather than directional spreading. This property of the micropatterns could be used to fine-tune cell shape and hence cell fate decisions [46]. Although cell motility was not monitored in this study, directional cell spreading is associated with more rapid and directional cell migration on micropatterned substrates [47]. This could be related to the increased extension of lamellipodia in cell regions exerting higher tractional forces [48]. We similarly observed high levels of membrane ruffling at cell edges extending on peptide spots away from the cell center (Movie 3). The RGD micropatterning density could therefore be adjusted to modify the rate of cell migration. After 3 days of cell expansion, the micropatterns ceased to critically impact the localization of focal adhesions, suggesting endogenous ECM deposition by the HSVECs after 3 days. The aerosol micropatterning technique using RGD and WQPPRARI therefore offers a simple means to modify cell shape and events occurring during the first few hours of cell-substrate interaction without affecting FAK activation or cell expansion at later time points.

In our previous studies, PTFE micropatterned with surface-conjugated GRGDS and WQPPRARI peptides significantly improved bovine aortic endothelial cell [22] and human umbilical vein endothelial cell [24] expansion. Similar results were obtained for human pulmonary aortic endothelial cells grown on surfactant polymers functionalized with a mixture of RGD and WQPPRARI peptides [49]. Conversely, the current results did not indicate any significant differences in HSVEC expansion between uniform and micropatterned GRGDS:WQPPRARI surface treatment. We previously reached the same conclusion for HSVEC expansion on PTFE at most time points examined although the peptide surface density in these experiments was higher, at ~0.9 peptides/nm^2 [25]. The micropatterns also did not significantly improve cell spreading or FAK activation. The results obtained both on the micropatterned and on uniformly-treated surfaces indicated no significant synergistic effects between the WQPPRARI and RGD peptides on cell adhesion, FAK activation or cell expansion. Surfaces reacted with WQPPRARI alone did lead to cell spreading, focal adhesion formation and FAK activation as suggested by previous reports [13,24], albeit at lower levels than the RGD peptides. The WQPPRARI sequence is derived from the heparin-binding type III repeat region 14 of fibronectin. This sequence binds heparansulfate proteoglycans including syndecans through electrostatic interactions [50,51], and also binds the a4b1 integrin [50]. Syndecans cooperate with integrins to bind and reorganize the ECM [52]. The lack of effects of the RGD:WQPPRARI micropatterns on HSVEC expansion could therefore be explained by differences in integrin or syndecan subtypes expressed by different endothelial cell types [53]. Further optimization of the peptide micropatterning strategy could therefore benefit from analyzing the expression patterns and post-translational modifications [54] of heparan-sulfate proteoglycans, integrins and other surface receptors in different endothelial cell subtypes. The surface modification strategy could then be adapted to targeted cell types that should be recruited to the prostheses, such as endothelial progenitor cells. Micropatterning with two or several peptides could help tailor the surfaces to promote the adhesion and expansion of several cell types, such as endothelial progenitor cells as well as the desired mature endothelial cell progeny.

FAK was activated on all peptide-modified surfaces, particularly on all surfaces reacted with RGD-TAMRA. FAK phosphorylation is activated upon integrin clustering and maintained by cytoskeletal contraction through Rho activation. Highly spread cells such as those observed on RGD-TAMRA have high levels of cell contraction, which is associated with the activation of cell growth [16]. Several signaling cascades activated upon FAK Y397 phosphorylation play a key role in promoting cell spreading, motility and proliferation. FAK and its targets also play a crucial role in normal vascular development and angiogenesis [55]. This led us to test whether the RGDTAMRA modified surfaces could support the expansion of HSVECs in the absence of serum. To our knowledge, there are currently no commercially available serum-free media allowing primary human endothelial cell expansion in defined conditions. We modified a commercially available medium containing 1% serum by replacement with insulin, transferrin, selenium and BSA, leading to fully defined culture

conditions except for the non-recombinant BSA. Similar levels of HSVEC expansion were observed on RGD-TAMRA treated surfaces and collagen. Furthermore, HSVEC morphology and focal adhesion distributions were similar between RGD-TAMRA and collagen surfaces in serum-free medium, albeit fewer large mature focal adhesions were observed compared to control cultures with 20% serum. The significant cell expansion observed after 3 days on RGD-TAMRA is a promising basis for testing long-term primary endothelial cell expansion in defined conditions. The serum-free medium could be further optimized through the addition of other biomimetic peptides or soluble growth factors.

Promising avenues to improve the clinical potential of the aerosol-based micropatterning strategy include testing micropattern effects on cells exposed to physiological wall shear stress. For example, it would be interesting to compare the aerosol-generated patterns with linear GRGDS:WQPPRARI micropatterns that enhanced flow-induced cell reorientation [56]. The aerosol-generated micropatterns could also facilitate the large-scale production of micropatterned surfaces for therapeutic cell production.

The non-uniform cell microenvironment produced by micropatterned ECM molecules can significantly impact stem cell fate decisions [16]. For example, different shapes or sizes of micropatterned cell-adhesive substrates on non-adhesive backgrounds determine the differentiation pathways activated in mesenchymal stem cells. The anisotropic distribution of the aerosol-generated patterns could impact whether stem cells undergo symmetric or asymmetric cell division. In the context of vascular surgeries, micropatterned fibronectin-derived peptides could help recruit endothelial progenitor cells to vascular graft surfaces and control endothelial progenitor cell fate decisions [57], similar to fibronectin.

5 CONCLUSIONS

Vascular graft surface modification using biomimetic peptides could improve their long-term performance by creating a microenvironment more conducive to graft endothelialisation. Micropatterning of these peptides could better replicate the micron-scale anisotropic distribution of ECM proteins observed in fibrillar matrices. Aerosol-based peptide micropatterning is a simple technique that could be adapted to functionalize tubular structures or large surface areas. Aerosol-generated GRGDS:WQPPRARI micropatterns significantly increased endothelial cell adhesion and expansion compared to untreated surfaces. Surfaces reacted with mixtures of the two peptides led to uniform cell spreading, whereas the micropatterns led to directional cell spreading determined by the location of the micropatterns. Lastly, a fluorophore-tagged RGD peptide allowed real-time monitoring of micropattern effects on endothelial cells. This RGD-TAMRA peptide significantly increased cell spreading and FAK activation, in addition to allowing primary endothelial cell expansion in serum-free medium.

ACKNOWLEDGMENTS

The authors thank Marie-Claude Boivin, Jérôme Noël, Mathias Mangion, Simon Asselin-Tardif and Mariève Boulanger for technical support (all at Université Laval and the Centre de Recherche du CHU de Québec). Mariève Boulanger also participated in manuscript proof-reading. We also thank Dr Bruno Gaillet (Université Laval) and Dr Tim Allsopp (Neusentis, Pfizer Ltd) for useful discussions. Financial support was provided by a See the Potential postdoctoral fellowship from Pfizer Ltd and Pfizer Canada Inc and the Canadian Stem Cell Network (CH), by a non-restricted grant from Pfizer Ltd (CH, AG and GL), by the Canadian Natural Sciences and Engineering Research Council (Discovery Grant and CREATE programs, GL), by the Centre Québécois sur les Matériaux Fonctionnels (GL) and by the Canada Foundation for Innovation (CD).

REFERENCES

[1] Klinkert P, Post PN, Breslau PJ, van Bockel JH. Saphenous vein versus PTFE for above-knee femoropopliteal bypass. A review of the literature. Eur J Vasc Endovasc Surg 2004;27(4):357e62.

[2] Meinhart JG, Deutsch M, Fischlein T, Howanietz N, Froschl A, Zilla P. Clinical autologous in vitro endothelialization of 153 infrainguinal ePTFE grafts. Ann Thorac Surg 2001;71(5 Suppl.):S327e31.

[3] Laube HR, Duwe J, Rutsch W, Konertz W. Clinical experience with autologous endothelial cell-seeded polytetrafluoroethylene coronary artery bypass grafts. J Thorac Cardiovasc Surg 2000;120(1):134e41.

[4] Vara DS, Salacinski HJ, Kannan RY, Bordenave L, Hamilton G, Seifalian AM. Cardiovascular tissue engineering: state of the art. Pathol Biol (Paris) 2005;53(10):599e612.

[5] Meinhart JG, Schense JC, Schima H, Gorlitzer M, Hubbell JA, Deutsch M, et al. Enhanced endothelial cell retention on shear-stressed synthetic vascular grafts precoated with RGD-cross-linked fibrin. Tissue Eng 2005;11(5e6):887e95.

[6] Fernandez P, Bareille R, Conrad V, Midy D, Bordenave L. Evaluation of an in vitro endothelialized vascular graft under pulsatile shear stress with a novel radiolabeling procedure. Biomaterials 2001;22(7):649e58.

[7] Feugier P, Black RA, Hunt JA, How TV. Attachment, morphology and adherence of human endothelial cells to vascular prosthesis materials under the action of shear stress. Biomaterials 2005;26(13):1457e66.

[8] Li JM, Menconi MJ, Wheeler HB, Rohrer MJ, Klassen VA, Ansell JE, et al. Precoating expanded polytetrafluoroethylene grafts alters production of endothelial cell-derived thrombomodulators. J Vasc Surg 1992;15(6):1010e7.

[9] George EL, Baldwin HS, Hynes RO. Fibronectins are essential for heart and blood vessel morphogenesis but are dispensable for initial specification of precursor cells. Blood 1997;90(8):3073e81.

[10] Astrof S, Hynes RO. Fibronectins in vascular morphogenesis. Angiogenesis 2009;12(2):165e75.

[11] Serini G, Valdembri D, Bussolino F. Integrins and angiogenesis: a sticky business. Exp Cell Res 2006;312(5):651e8.

[12] Midwood KS, Mao Y, Hsia HC, Valenick LV, Schwarzbauer JE. Modulation of cell-fibronectin matrix interactions during tissue repair. J Investig Dermatol Symp Proc 2006;11(1):73e8.

[13] Mooradian DL, McCarthy JB, Skubitz AP, Cameron JD, Furcht LT. Characterization of FN-C/H-V, a novel synthetic peptide from fibronectin that promotes rabbit corneal epithelial cell adhesion, spreading, and motility. Invest Ophthalmol Vis Sci 1993;34(1):153e64.

[14] Huebsch JC, McCarthy JB, Diglio CA, Mooradian DL. Endothelial cell interactions with synthetic peptides from the carboxyl-terminal heparin-binding domains of fibronectin. Circ Res 1995;77(1):43e53.

[15] Peters DMP, Chen Y, Zardi L, Brummel S. Conformation of fibronectin fibrils varies: discrete globular domains of type III repeats detected. Microsc Microanal 1998;4(4):385e96.

[16] Thery M. Micropatterning as a tool to decipher cell morphogenesis and functions. J Cell Sci 2010;123(24):4201e13.

[17] Chen CS, Mrksich M, Huang S, Whitesides GM, Ingber DE. Geometric control of cell life and death. Science 1997;276(5317):1425e8.

[18] Guillou H, Depraz-Depland A, Planus E, Vianay B, Chaussy J, Grichine A, et al. Lamellipodia nucleation by filopodia depends on integrin occupancy and downstream Rac1 signaling. Exp Cell Res 2008;314(3):478e88.

[19] Lehnert D, Wehrle-Haller B, David C, Weiland U, Ballestrem C, Imhof BA, et al. Cell behaviour on micropatterned substrata: limits of extracellular matrix geometry for spreading and adhesion. J Cell Sci 2004;117(Pt 1):41e52.

[20] Norman JJ, Desai TA. Methods for fabrication of nanoscale topography for tissue engineering scaffolds. Ann Biomed Eng 2006;34(1):89e101.

[21] Whitesides GM, Ostuni E, Takayama S, Jiang X, Ingber DE. Soft lithography in biology and biochemistry. Annu Rev Biomed Eng 2001;3:335e73.

[22] Gagne L, Rivera G, Laroche G. Micropatterning with aerosols: application for biomaterials. Biomaterials 2006;27(31):5430e9.

[23] Boivin MC, Chevallier P, Turgeon S, Lagueux J, Laroche G. Micropatterning polymer materials to improve endothelialization. Adv Mat Res 2011;409: 777e82 [THERMEC 2011 Supplement].

[24] Gauvreau V, Laroche G. Micropattern printing of adhesion, spreading, and migration peptides on poly(tetrafluoroethylene) films to promote endothelialization. Bioconjug Chem 2005;16(5):1088e97.

[25] Boivin MC, Chevallier P, Hoesli CA, Lagueux J, Bareille R, Remy M, et al. Human saphenous vein endothelial cell adhesion and expansion on micropatterned polytetrafluoroethylene. J Biomed Mater Res A 2013;101(3):694e703.

[26] Vallieres K, Petitclerc E, Laroche G. Covalent grafting of fibronectin onto plasma-treated PTFE: influence of the conjugation strategy on fibronectin biological activity. Macromol Biosci 2007;7(5):738e45.

[27] Juneau P-M, Garnier A, Duchesne C. Selection and tuning of a fast and simple phase-contrast microscopy image segmentation algorithm for measuring myoblast growth kinetics in an automated manner. Microsc Microanal 2013: 1e12. FirstView.

[28] Lagergren S. Zur theorie der sogenannten adsorption gelöster stoffe. Kungliga Svenska Vetenskapsakademiens; 1898. Handlingar.

[29] Xue Y, O'Mara ML, Surawski PP, Trau M, Mark AE. Effect of poly(ethylene glycol) (PEG) spacers on the conformational properties of small peptides: a molecular dynamics study. Langmuir 2011;27(1):296e303.

[30] Horton MA, Dorey EL, Nesbitt SA, Samanen J, Ali FE, Stadel JM, et al. Modulation of vitronectin receptor-mediated osteoclast adhesion by Arg-Gly-Asp peptide analogs: a structure-function analysis. J Bone Miner Res 1993;8(2):239e47.

[31] Gagne L, Laroche G. Engineering biomaterials surfaces using micropatterning. Adv Mat Res 2007;15e17:77e82 [THERMEC 2006 Supplement].

[32] Schwarzbauer JE, DeSimone DW. Fibronectins, their fibrillogenesis, and in vivo functions. Cold Spring Harb Perspect Biol 2011;3(7).

[33] Pompe T, Renner L, Werner C. Nanoscale features of fibronectin fibrillogenesis depend on protein-substrate interaction and cytoskeleton structure. Biophys J 2005;88(1):527e34.

[34] Maheshwari G, Brown G, Lauffenburger DA, Wells A, Griffith LG. Cell adhesion and motility depend on nanoscale RGD clustering. J Cell Sci 2000;113(Pt 10): 1677e86.

[35] Comisar WA, Mooney DJ, Linderman JJ. Integrin organization: linking adhesion ligand nanopatterns with altered cell responses. J Theor Biol 2011;274(1):120e30.

[36] Cavalcanti-Adam EA, Volberg T, Micoulet A, Kessler H, Geiger B, Spatz JP. Cell spreading and focal adhesion dynamics are regulated by spacing of integrin ligands. Biophys J 2007;92(8):2964e74.